Ndm, a coiled-coil domain protein that suppresses macropinocytosis and has effects on cell migration

Jessica S. Kelsey, Nathan M. Fastman, Elizabeth F. Noratel, and Daphne D. Blumberg
Department of Biological Sciences, University of Maryland, Baltimore County, Baltimore, MD 21250

ABSTRACT The *ampA* gene has a role in cell migration in *Dictyostelium discoideum*. Cells overexpressing AmpA show an increase in cell migration, forming large plaques on bacterial lawns. A second-site suppressor of this *ampA*-overexpressing phenotype identified a previously uncharacterized gene, *ndm*, which is described here. The Ndm protein is predicted to contain a coiled-coil BAR-like domain—a domain involved in endocytosis and membrane bending. *ndm*-knockout and Ndm-monomeric red fluorescent protein–expressing cell lines were used to establish a role for *ndm* in suppressing endocytosis. An increase in the rate of endocytosis and in the number of endosomes was detected in *ndm⁻* cells. During migration *ndm⁻* cells formed numerous endocytic cups instead of the broad lamellipodia structure characteristic of moving cells. A second lamellipodia-based function—cell spreading—was also defective in the *ndm⁻* cells. The increase in endocytosis and the defect in lamellipodia formation were associated with reduced chemotaxis in *ndm⁻* cells. Immunofluorescence results and glutathione *S*-transferase pull-down assays revealed an association of Ndm with coronin and F-actin. The results establish *ndm* as a gene important in regulating the balance between formation of endocytic cups and lamellipodia structures.

INTRODUCTION

The dynamic organization of the actin cytoskeleton is essential in the processes of cell migration and endocytosis. Chemotaxing cells sense environmental signals and coordinate the actin cytoskeleton for directed movements. Activation of chemoattractant receptors recruits proteins to sites of actin polymerization within the cell, causing polarization. These proteins include phospholipid kinases and phospholipases, which affect membrane lipid composition, as well as Rac GTPases (a subset of the Rho family of GTPases), which regulate actin cytoskeleton assembly (Affolter and Weijer, 2005). The enrichment in membrane phospholipids and the increase in Rac GTPases in the front of the moving cell attract and activate other actin-associating proteins, promoting the assembly of pseudopods (Insall and Machesky, 2009).

Actin organization is essential in the endocytic process as well (Girao *et al.*, 2008). Receptor-mediated endocytosis uses actin polymerization during clathrin-coated pit formation and endocytic vesicle budding (Collins *et al.*, 2011). The uptake of particles—phagocytosis—occurs with the assistance of an actin-rich endocytic cup (May and Machesky, 2001). During the actin-driven process of macropinocytosis, actin-rich ruffles extend from the cell (Hacker *et al.*, 1997). These ruffles can form into actin-rich endocytic cups, coordinating bulk fluid-phase uptake into the cell.

Actin-binding proteins regulate actin filament formation, permitting prompt and accurate organization for the variety of cellular processes. The Arp2/3 complex binds actin and is a powerful actin nucleator; it promotes branching of the filaments (Machesky *et al.*, 1997; Machesky and Insall, 1998; Insall *et al.*, 2001). The actin-binding protein coronin interacts with the Arp2/3 complex and is suggested to have dynamic roles in actin filament assembly; it is suggested to act in protecting new areas of filament assembly and
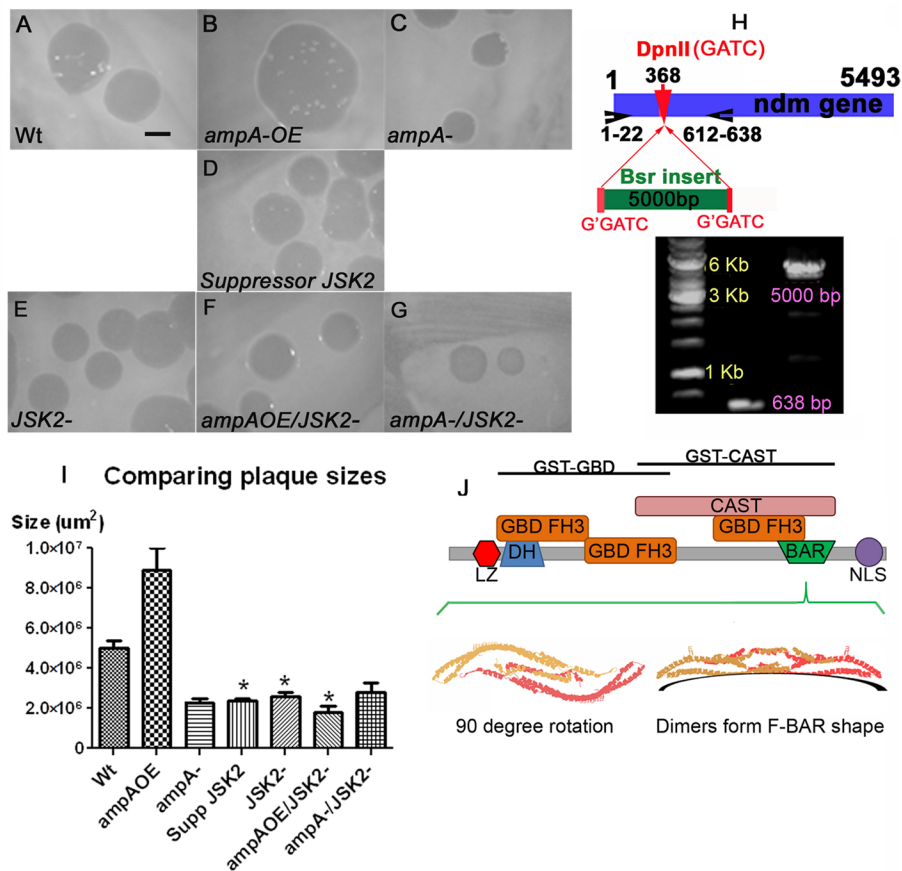
FIGURE 1: JSK2 plaque sizes indicate suppression of the *ampOE* phenotype. (A–G) Wild-type (WT), *ampA*, and *JSK2* mutant plaques. The average areas are graphed in I. Plates were incubated at 22°C for 4 d. Scale bar, 1000 μm. $n = 15+$ plaques from at least three independent experiments. Error bars in I are SEM. *$p < 0.05$, indicating a significant difference between WT or AmpA OE and their respective *JSK2⁻* mutants. A p value of 0.88 indicating no significant difference was found when comparing *ampA⁻* plaque sizes with *amp⁻/JSK2⁻* plaque sizes. (H) Top, a diagram showing the insertion site of the REMI plasmid containing the blasticidin resistance cassette (bsr) into the *ndm* gene. It was inserted at the *Dpn*II (GATC) site at base pair 368 via the complementary sites created by *Bam*HI digestion (G'GATC). The black arrows show primer locations for PCR. Bottom, PCR analysis using primers flanking the predicted REMI plasmid insertion site shows a shift in product from 638 base pairs in WT DNA to 5000 base pairs in *JSK2⁻* DNA, confirming disruption of the *JSK2⁻* gene. J, protein domains predicted by the MotifScan program are indicated with amino acid positions (Pagni *et al.*, 2007). LZ (leucine zipper), DH (double homology), GBD-FH3 (G-protein–binding formin homology 3), CAST (region of homology to the CAST protein), BAR (BAR domain), and NLS (nuclear localization signal). Black bars indicate the protein regions used in GST fusions. A model of the BAR domain is shown below (I-TASSER; Roy *et al.*, 2010). Images are of dimers, with one BAR domain in orange and one in pink. Left, a view rotated 90°. Right, the dimer attached to a curved membrane, where the characteristic F-BAR domain curvature is evident.

increasing filament disassembly in older areas (de Hostos, 1999; Humphries *et al.*, 2002; Gandhi *et al.*, 2009).

In addition to actin dynamics, membrane dynamics is an essential component in the formation of cellular processes and changes in cell shape (Graham and Kozlov, 2010). Membrane-interacting proteins regulating membrane dynamics during endocytosis, vesicle trafficking, and formation of cell protrusions are crucial. An important class of membrane-associating proteins comprises membrane-bending, BAR domain–containing proteins.

The coiled-coil BAR domain is highly diverged, with little sequence similarity between proteins. The structural folding of the proteins is the defining element (Salazar *et al.*, 2003; Frost *et al.*, 2009; Prendergast *et al.*, 2009; Campos-Parra *et al.*, 2010; Suetsugu,

2010). The BAR superfamily is divided into subfamilies according to the curvature that the domains exhibit. The classic BAR domain has a concave shape. The F-BAR domain has a concave, crescent shape, but the curvature is shallower than that of the classic BAR domain. The I-BAR domain has a convex curvature. Although the BAR proteins are best known for their functions in endocytosis, they have also been shown to be involved in vesicle trafficking, cell division, cell polarity, and migration, as well as in transcription and tumor suppressor activity. A number of human diseases are associated with mutations in BAR-containing proteins. These include Alzheimer's disease, diabetes, mental retardation, and bladder and prostate carcinoma, which underscore the impact of the BAR domain (Frost *et al.*, 2009).

In this article, we describe a novel multi-domain protein, Ndm, which contains a coiled-coil, C-terminal BAR-like domain and acts to suppress macropinocytosis. It associates with vesicles and colocalizes with proteins involved in cytoskeletal organization such as coronin. Ndm protein interaction with the cytoskeleton appears to be important for cell spreading and cell migration, as knockouts show defects in chemotaxis and cell spreading. Ndm was identified in a screen for suppressors of a cell strain that overexpresses the AmpA protein in *Dictyostelium discoideum*. AmpA is expressed in growing cells, where it functions to increase actin polymerization and promote cell migration (Blumberg *et al.*, 2002; Casademunt *et al.*, 2002; Varney *et al.*, 2002a,b).

The amoeba *D. discoideum* is an attractive model system for studying dynamic actin-based processes (Soll, 2003; Janetopoulos and Firtel, 2008; Noegel and Schleicher, 2000). Our characterization of Ndm identifies a new protein necessary for the formation of rounded lamellipodial structures and that suppresses the formation of endocytic cups.

RESULTS

Identification of a suppressor of the *ampAOE* large-plaque phenotype

When *Dictyostelium* cells are plated on lawns of bacteria they consume the bacteria as they migrate further out into the lawn, creating a clearing called a plaque. AmpA-overexpressing (*ampAOE*) cells produce plaques that are larger than WT cells. *AmpA*-null cells produce very small plaques (Figure 1, A–C and I). The differences in plaque size are likely due to differences in migration since neither phagocytosis nor growth rate is significantly altered in these strains. A difference in migration rate of cells as a function of AmpA levels has been observed (unpublished data). Restriction enzyme–mediated integration (REMI) mutagenesis was used to obtain mutants that suppress the *ampAOE* large-plaque phenotype. REMI mutagenesis involves the random insertion of a linearized blasticidin-resistant cassette (bsr)–containing plasmid into

the *Dictyostelium* genome. More than 6000 REMI mutants were screened for their ability to suppress the large-plaque *ampAOE* phenotype, and three mutants were identified and characterized for their suppressing ability (JSK1, JSK2, and JSK3). This article focuses on the identification and characterization of the *JSK2* gene. The gene disrupted by the JSK2 mutant was identified as an uncharacterized gene, DDB_G0272368, by sequencing the DNA flanking the inserted REMI plasmid. The *JSK2* mutant (Figure 1, D and I) produced much smaller plaques than the *ampAOE* (Figure 1, B and I). To confirm that the insertion into DDB_G0272368 was responsible for the suppression of plaque size, the REMI plasmid was recovered and used to generate an independent knockout in *ampAOE* cells, as well as in WT and *ampA*-null cells. These cell lines all consistently produced small plaques on bacterial lawns (Figure 1, E–G and I). A double-knockout mutant in both *JSK2* and *ampA* was created to determine whether there was involvement of the suppressor gene in the *ampA* pathway. The plaque sizes of the double mutant were not significantly different from those of either mutant alone, suggesting that *JSK2* and *ampA* might be involved in the same pathway controlling plaque size (Figure 1, C, E, G, and I). A double knockout of genes in different pathways usually results in an additive effect, which should have been visible as a much smaller plaque. PCR using primers flanking the insertion site of the REMI plasmid confirmed the correct insertion of the REMI plasmid into the DDB_G0272368 gene in the wild-type strain, which is used subsequently to further characterize this gene (Figure 1H).

The DDB_G0272368 gene is predicted to contain a variety of domains, including BAR and CAST domains

The DDB_G0272368 gene is predicted to produce a 209-kDa, 1781–amino acid protein product. Based on protein prediction programs, the all-helical, coiled-coil structure was found to resemble importin/exportins, which traffic cargo into and out of the nucleus. The structure is also similar to AP2, a clathrin adapter protein important in vesicle formation and trafficking (Roy *et al.*, 2010). Although blast searches mainly revealed homology to coiled-coil domain–containing proteins, low homology similarity to a number of other protein domains was predicted by the MotifScan program (ExPASy Bioinformatics Resource Portal [http://expasy.org/]; Figure 1J). Among these are a leucine zipper domain, a double homology domain (DH), G-binding formin 3 homology domains (GBD-FH3), a CAST protein domain, a BAR domain, and a nuclear localization signal. Leucine zipper regions are involved in protein–protein interactions and are often found in transcription factors (Nikolaev and Pervushin, 2009). The GBD-FH3 domain is a low-sequence-homology N-terminal domain found in fungal and metazoan formins. Formins are actin-binding proteins that promote the formation of linear filaments. The FH3 domain appears to be responsible for targeting proteins (Petersen *et al.*, 1998; Rivero *et al.*, 2005). This region of formins has been shown to interact with Rho GTPases through a weakly defined G-binding domain that coincides with the FH3 domain. Rho GTPases are best known for their regulation of actin dynamic processes (Rivero and Somesh, 2002). The DH domain predicted in DDB_G0272368 is found in the Rho GTPase–regulating proteins (RhoGEFs). The DH regions are the sites of nucleotide exchange activity (Rivero *et al.*, 2005). Most RhoGEFs also contain a Pleckstrin homology (PH) domain, which allows association with membranes. A few exceptions to this are DH-containing proteins that also contain BAR domains instead of PH domains. It seems likely the membrane-associating BAR domain can take the place of the PH domain in such instances (Salazar *et al.*, 2003). To obtain further information on the BAR domain, we submitted its sequence

to a modeling program (Figure 1J). The BAR domain is predicted to belong to the F-BAR–domain subfamily of BAR-containing proteins. Its structure is most similar to the F-BAR-containing pascin/syndapin protein (Wang *et al.*, 2009). The CAST domain is a region similar to the CAST protein (also known as ELKS); it is a glutamine, leucine, lysine, and serine–rich Rab-interacting protein involved in vesicle trafficking and neurotransmitter release (Deken *et al.*, 2005; Kaeser *et al.*, 2009).

Disruption of the DDB_G0272368 gene results in increased endocytosis

A significant increase in endocytosis of fluorescein isothiocyanate (FITC)–labeled dextran was seen when DDB_G0272368 was disrupted in vegetative cells growing in shaking suspension (Figure 2A). This increase appeared to be specific to endocytosis, as exocytosis and phagocytosis were unchanged (Supplemental Figure S1). This suggests that the DDB_G0272368 gene functions to suppress endocytosis.

To determine whether the increase in endocytosis was due to an increased rate of uptake or formation of larger endocytic cups that could endocytose a larger volume, we characterized the endosomes (Figure 2, B and C). An increase in FITC-labeled dextran in early endosomes was observed in DDB_G0272368-knockout cells compared with WT cells (Figure 2B). Quantification of the amount of labeled dextran in the cells shows that there was a threefold increase in the amount of dextran in the DDB_G0272368 knockouts compared with WT (Figure 2C). Closer observation of the endosomes indicated that there were three times more endosomes in the DDB_G0272368-knockout cells, but the size of the endosomes was unchanged (Figure 2C). A similar result was seen when antibody to the p80 protein was used to visualize endosomes. The p80 protein specifically associates with endosomes and thus serves as a marker for them (Ravanel *et al.*, 2001). Disruption of the DDB_G0272368 gene results in a threefold increase in p80-containing endosomes (Figure 2, D–E).

Formation of endocytic cups by live wild-type and DDB_G0272368-knockout cells was also examined using time-lapse videomicroscopy. The cells were transformed with the green fluorescent protein (GFP)–filABD plasmid, which carries an F-actin–binding domain fused to GFP to enable visualization of F-actin dynamics (Washington and Knecht, 2008). It is clear from the videos (Supplemental Movies S1 and S2) that more endocytic cups form on the DDB_G0272368-knockout cells per unit time than on wild-type cells. Taken together, these results suggest that the knockout cells are carrying out endocytosis at a greater rate by forming more cups. Due to the defect seen when DDB_G0272368 is knocked out, the gene was named *ndm*, for negative director of macropinocytosis.

ndm knockout affects cell spreading

Because actin polymerization activity is needed for macropinocytosis, effects of *ndm* knockout on the actin cytoskeleton were investigated (Hacker *et al.*, 1997). When *ndm*⁻ cells were grown overnight on coverslips they were significantly taller than wild-type cells, suggesting an inability of the cells to spread properly (Figure 3A). When growing wild-type and *ndm*⁻ cells were initially deposited on coverslips and left in a growth chamber for 4 h or less, they were the same height, but after 12 h or more, *ndm*⁻ cells remained tall (average height of 13 µm, the same as at 4 h), whereas WT cells shortened and spread (average height of 7.5 µm after 12 h; Figure 3B). The increased cell height in *ndm*⁻ cells was accompanied by a decrease in cell perimeter at the base of the cell, further confirming the inability of the cells to spread properly (Figure 3C). The total volume
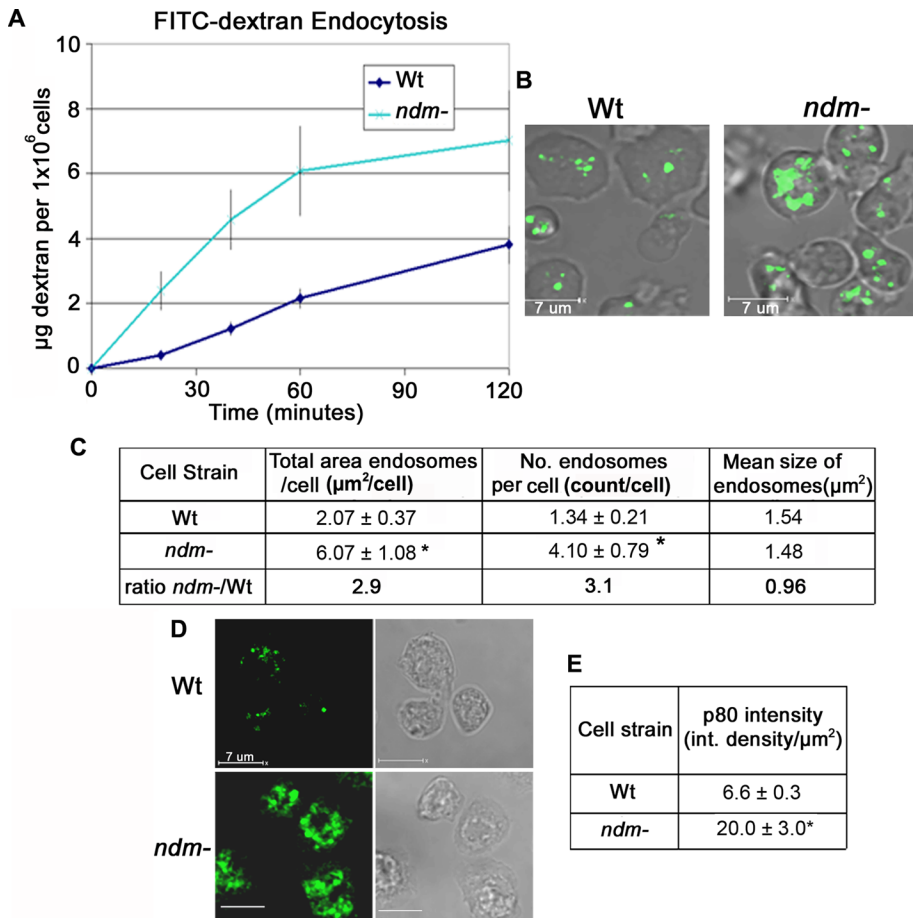
A FITC-dextran Endocytosis

FIGURE 2: Endocytosis is increased in *ndm⁻* cells. (A) FITC-dextran was used to measure rates of endocytosis (µg dextran/10⁶ cells) vs. time (min) in WT and *ndm⁻* cells (*n* = 3+ independent experiments). Error bars, SEM. (B) Cells displaying endosomes containing FITC-dextran. Images are optical sections with fluorescent and transmitted images overlaid. (C) Quantification of endosomes. The area of total endosomes/cell (µm²/cell) was measured using total area of FITC fluorescence/cell. The number of dextran-containing vesicles (number of endosomes/cell) was calculated by quantifying the number of individual FITC-containing endosomes/cell. Only spots large enough to be endosomes (not much smaller than 1.6 µm²) were counted. The size of the endosomes was unaffected (mean size of endosomes, µm²). (D) Antibody to the p80 protein (green) was used to label endosomes. A corresponding transmitted image is also displayed. (E) The amount of immunofluorescence in p80 endosomes is shown. In C and E, *$p < 0.05$ (*n* = 30+ cells, at least three independent experiments).

of *ndm⁻* and WT cells growing overnight on coverslips was the same, indicating that the greater height of *ndm⁻* cells was due to a defect in cell spreading and not a change in cell volume (Figure 3C). The failure of the *ndm⁻* cells to spread was not due to differences in substrate adhesion, because both wild-type and *ndm⁻* cells show no differences in substrate adhesion assays (Supplemental Figure S1). The inability of a cell to spread can be the result of a defect in formation of F-actin–rich lamellipodia (Chamaraux et al., 2005). Because F-actin–based protrusions are important in cell migration, as well as in cell spreading, we analyzed the motility of *ndm⁻* cells.

The *ndm⁻* mutants cannot extend smooth, rounded pseudopods, and they show defects in cell migration

WT and *ndm⁻* cells were allowed to migrate toward folic acid and were then fixed and stained for F-actin with phalloidin. The polymerized actin organization in the pseudopods of the *ndm⁻* cells was remarkably different from that of WT cells (Figure 4A). Pseudopods of *ndm⁻* cells appeared to break up into what looked like multiple en-

docytic cups instead of the smooth pseudopods characteristic of wild-type cells. A large number of actin-rich endocytic cups were seen extending from all areas of *ndm⁻* cells, with the greatest concentration in the front of the moving cell. This characteristic was also seen in live cells as they chemotaxed toward folic acid (Figure 4B). The WT cells displayed a fairly broad and consistent amount of extension. The *ndm⁻* cells produced regions of extensions that then broke up into smaller protrusions like endocytic cups.

Dictyostelium cells use folic acid produced by bacteria as a chemoattractant. Chemotaxis of *ndm⁻* cells to folic acid was compared with that of WT cells (Figure 4, C–E). The rate of movement (velocity) appeared unchanged in *ndm⁻* cells migrating to folic acid (Figure 4E). Compared to WT cells, *ndm⁻* cells displayed a slight but significant ($p < 0.05$) decrease in the ability of the cell to travel in a straight path (directionality; the Euclidean distance moved from the start of imaging to the end point divided by the total distance moved over the time of the assay; Figure 4E). Most strikingly, there was a significant decrease in the chemotactic index in *ndm⁻* cells, which, as described in *Materials and Methods*, is a measure of movement in the direction of the chemoattractant (Figure 4E). Chemotaxis plots demonstrate this impairment in *ndm⁻* cells, showing many cells moving away from the chemoattractant rather than toward it (Figure 4, C and D). This is in contrast to the WT cells, which traveled mostly in the direction of the chemoattractant. Developing *ndm⁻* cells migrating to cAMP also had a significant decrease in their chemotactic index compared with WT cells (Figure 4E), with many *ndm⁻* cells migrating away from the cAMP source. The defect in chemotaxis in *ndm⁻* cells is likely the reason why *ndm⁻* cells produce small plaques on lawns of bacteria. It is possible that the increased amount of endocytosis and defective lamellipodia formation affects the ability of the cells to detect the chemoattractant.

ndm expression is influenced by cell density and is necessary in development

To further understand the role of *ndm* in endocytosis and actin organization, an Ndm–monomeric red fluorescent protein (mRFP) fusion protein construct was generated in order to determine the localization of *ndm* in the cell. The plasmid containing the *ndm*-mRFP fusion protein gene was knocked into wild-type cells and shown by PCR to have replaced the wild-type gene with the mRFP fusion construct (Supplemental Figure S2). In this construct the Ndm-mRFP fusion protein is driven by the Ndm promoter. The *ndm*-mRFP fusion protein was correctly expressed, and Ndm-mRFP–expressing cells retained wild-type phenotypes in growing cells. The Ndm-mRFP–expressing cells made wild-type-size plaques and showed wild-type amounts of endocytosis (Supplemental Figure S2). This
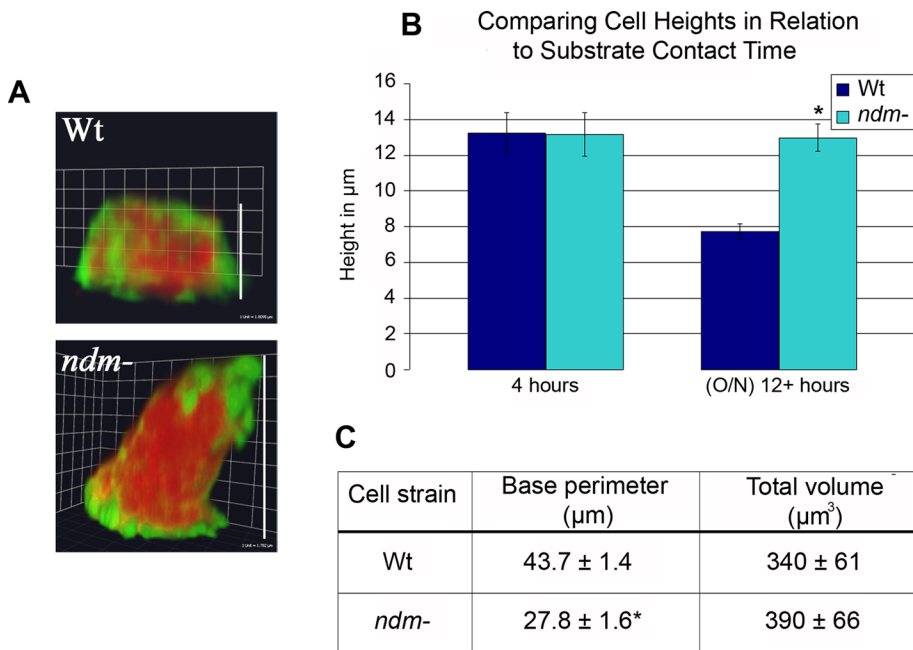
A

Wt

ndm-

B

Comparing Cell Heights in Relation to Substrate Contact Time

C

Cell strain	Base perimeter (µm)	Total volume (µm³)
Wt	43.7 ± 1.4	340 ± 61
ndm-	27.8 ± 1.6*	390 ± 66

FIGURE 3: The *ndm* knockout displays defects in cell spreading. (A) Three-dimensional (3D) reconstructed images of WT and *ndm⁻* cells after growing overnight on coverslips. F-actin (green) and G-actin (red). (B) WT and *ndm⁻* cell heights after 4 or >12 h of growing on coverslips ($n = 3$ independent experiments with 25+ cells per strain). Error bars, SEM. (C) Quantification of the perimeter at the base of the cells and the total volume of the cells for WT and *ndm⁻*. Volocity 3D measurement software was used to calculate cell volume from the distribution of TRITC-DNase I fluorescence staining of G-actin in cells. The base perimeter was determined from traces of the cell circumference in optical sections at the coverslip, and the height of the cells was determined by measuring from the coverslip to the top of individual cells on the z-axis. *$p < 0.05$; $n = 30+$ cells per cell strain.

indicated that in growing cells the Ndm-mRFP fusion protein could substitute for the wild-type Ndm protein and be used as a marker for the localization of the Ndm protein in growing cells.

Ndm was localized in punctate spots throughout the growing cells, with strong localization to the periphery (Figure 5A). With increasing density, the amount of Ndm protein decreased sharply, and the punctate signal decreased. A portion of the remaining Ndm protein appeared to localize more to the nucleus (Figure 5, A, B, and D). Pearson's coefficient values for colocalization with 4′,6-diamidino-2-phenylindole (DAPI) stain were determined (Figure 5B), and cell fractionations were done (Figure 5D). There was a significant increase in the correlation values in high-density cells compared with the low-density cells, but the positive correlation value was relatively low (only 0.3), indicative of the fact that only a small portion of the protein is nuclear in location. Fractionation results of Ndm-mRFP protein in low- and high-density cells show that at each density the majority of Ndm associates with membranes, suggesting that the dispersed punctate signal is the result of Ndm associated with membrane vesicles (Figure 5D). At high density, some protein was associated with the soluble nuclear fraction, consistent with the low amount of protein colocalizing with the nucleus in the immunofluorescence images. Although only a small portion of the Ndm protein appears to localize to the nucleus, the Ndm protein does have a nuclear localization signal (Figure 1J).

Reverse transcription (RT)-PCR analysis of mRNA transcripts indicates that *ndm* mRNA is at its highest level in growing cells, but it is also present during development (Figure 6, A and B). The mRNA level is very low during aggregation (4 h) but starts to reaccumulate, reaching a maximum at late mound stage (12 h). The time course of

accumulation of the Ndm-mRFP protein follows closely the accumulation of the *ndm* mRNA (Supplemental Figure S3). *ndm⁻* cells displayed a developmental defect, forming fewer and sparser developing structures (Figure 6C). Fruiting bodies appear smaller and weaker compared with WT (Figure 6C, 24 h). The Ndm-mRFP protein, which functions like wild type in growing cells, also rescues the sparseness of the field of developing structures during early development and is similar to wild type through 12 h, but it arrests development at mound stage and progresses no further (Figure 6C). The fact that after 12 h of development this construct causes developmental arrest suggests that it is acting as a dominant negative during late development. This suggests that *ndm* has a second target with which it interacts in developing cells that is negatively impacted by the presence of the mRFP tag, causing the fusion protein to act as a dominant negative. Thus the mRFP-tagged Ndm protein appears to be fully functional during growth and early development, but it is not a suitable tag for later developmental functions. Thus all of the studies that follow using this tag are carried out only in growing cells, where the Ndm-mRFP protein has wild-type function.

In vegetative cells, Ndm interacts with proteins involved in actin dynamic processes

Endocytosis and migration are actin-driven processes. Because *ndm* appears to be involved in both, Ndm was tested for interactions with endocytic or actin-associating proteins. Indirect immunofluorescence was used to determine localization of Ndm-mRFP relative to clathrin, coronin, and F-actin (Figure 7). Both growing cells sitting on coverslips (stationary) and growing cells migrating toward folic acid were compared, since some protein localizations might change during cell migration. Clathrin is involved in substrate internalization and vesicle formation, as well as in trafficking during endocytosis (O'Halloran and Anderson, 1992; Girao *et al.*, 2008). There was a positive correlation value (Figure 7D), and areas of overlap were apparent in both the stationary and migrating cells (Figure 7A). Coronin is an actin-binding protein involved in actin remodeling during the formation of endocytic processes and lamellipodial protrusions (Gerisch *et al.*, 1995; Hacker *et al.*, 1997; Mishima and Nishida, 1999; Uetrecht and Bear, 2006). Extensive colocalization was seen between Ndm-mRFP and coronin. A large amount of colocalization in stationary cells was detected (Figure 7B). In migrating cells Ndm and coronin colocalized at the cell poles, where actin-rich pseudopods would be forming. There was a high positive correlation, with a value of nearly 0.8, very close to a complete colocalization value of 1 (Figure 7D). *ndm⁻* phenotypes suggest its involvement in F-actin–dependent processes, and so it was not surprising to find Ndm-mRFP colocalizing with F-actin. Small areas of overlap between Ndm-mRFP and F-actin were seen in stationary cells, but a significant increase in association with actin is observed in migrating cells, where pseudopodial protrusions are important (Figure 7C). The *r* was low between Ndm and F-actin in stationary cells but was higher in migrating cells (Figure 7D). For
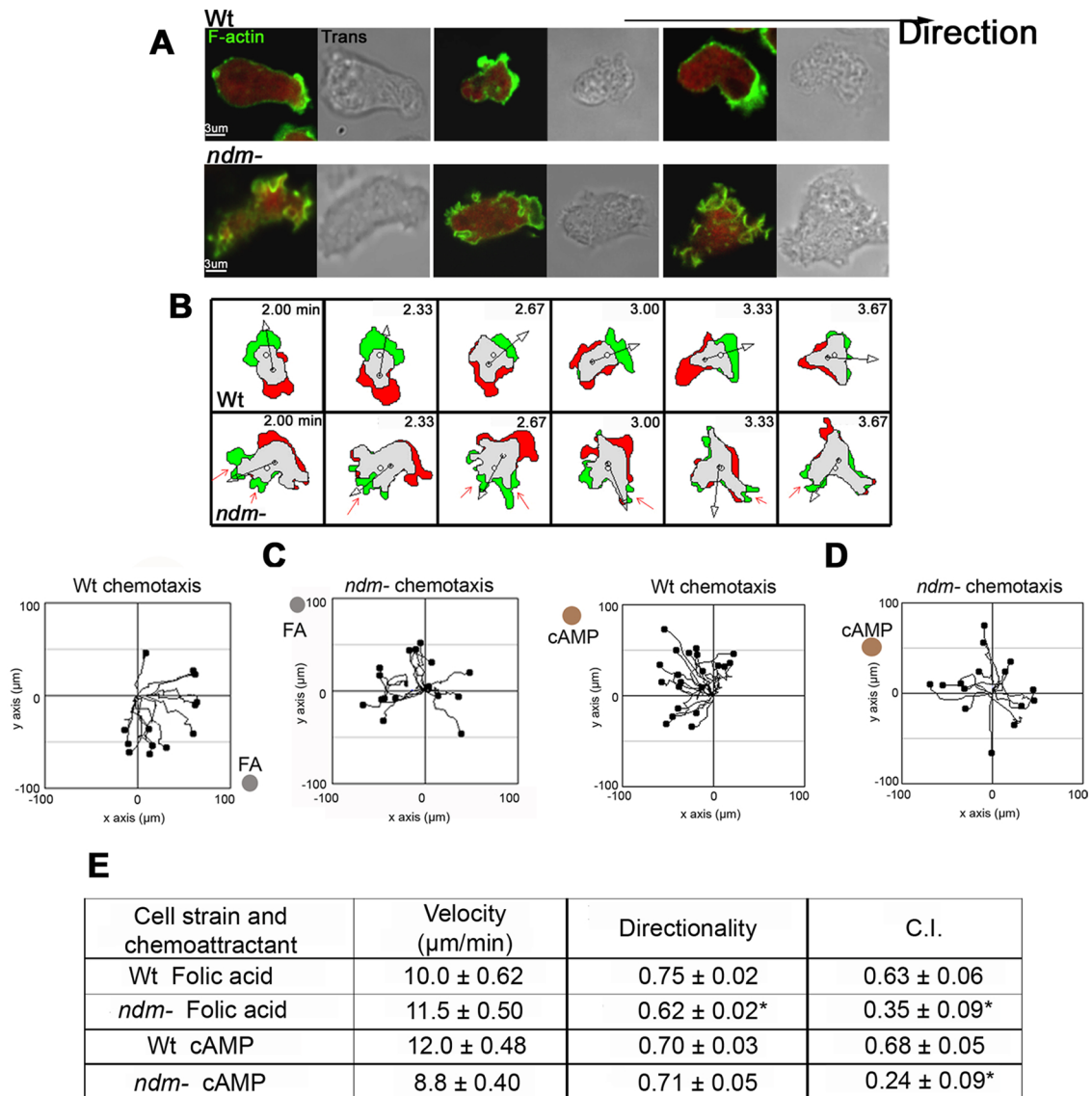
FIGURE 4: *ndm⁻* cells display defects in cell migration. (A) Cells chemotaxing toward folic acid on coverslips were fixed and stained for F-actin (green) and G-actin (red). Optical sections are shown next to transmitted images. Three WT cells (top) and three *ndm⁻* cells (bottom) are illustrated. (B–E) Cells on top of agar chemotaxing toward folic acid were imaged every 20 s. (B) Difference plots (Dynamic Image Analysis System; Solltech, Iowa City, IA). Top, WT cell; bottom, *ndm⁻* cell. Gray areas are regions that remain the same, green areas represent regions of extension from the previous panel, and red areas represent regions of retraction. (C, D) Chemotaxis plots of WT and *ndm⁻* cells migrating to (C) folic acid and (D) cAMP. Black dots represent cells. Individual paths >5 min are shown by black lines attached to each dot. The direction and distance of each cell from its origin at 0 are shown. The location of folic acid (FA) or cAMP is indicated by gray (FA) or brown (cAMP) dots. (E) Values for velocity, directionality, and CI of WT and *ndm⁻* cells chemotaxing toward folic acid or cAMP. *$p < 0.05$ ($n = 50+$ cells from at least three independent experiments). Calculation of CI is given in *Materials and Methods*.

comparison purposes, colocalization of Ndm with fimbrin, another actin-binding protein, was determined. Little colocalization between Ndm-mRFP and fimbrin was found, emphasizing that not all actin-binding proteins showed colocalization (unpublished data). Colocalization results shown are for low-density cells, when Ndm expression is at its maximum.

Because there was substantial overlap between Ndm and coronin in colocalization experiments, glutathione S-transferase (GST) pull-down experiments were undertaken to determine whether there were interactions between the proteins. The entire Ndm protein-coding region could not be maintained stably on bacterial plas-

mids in *Escherichia coli*, and so GST fusion proteins were constructed containing different smaller regions of the Ndm protein (indicated in Figure 1J). A GST-GBD fusion construct was made containing the first two GBD-formin 3 domains. In addition, a GST-CAST fusion construct that contains the CAST domain and the BAR domain was constructed. After incubation with cell lysates, F-actin and coronin were found to associate with the CAST-domain region of Ndm (Figure 8A). The association of coronin and actin with the CAST domain of Ndm was demonstrated by doing Western blots of the pulled-down proteins. In addition, bands running in the range of 55 and 45 kDa were excised from the gel-separated pull-down
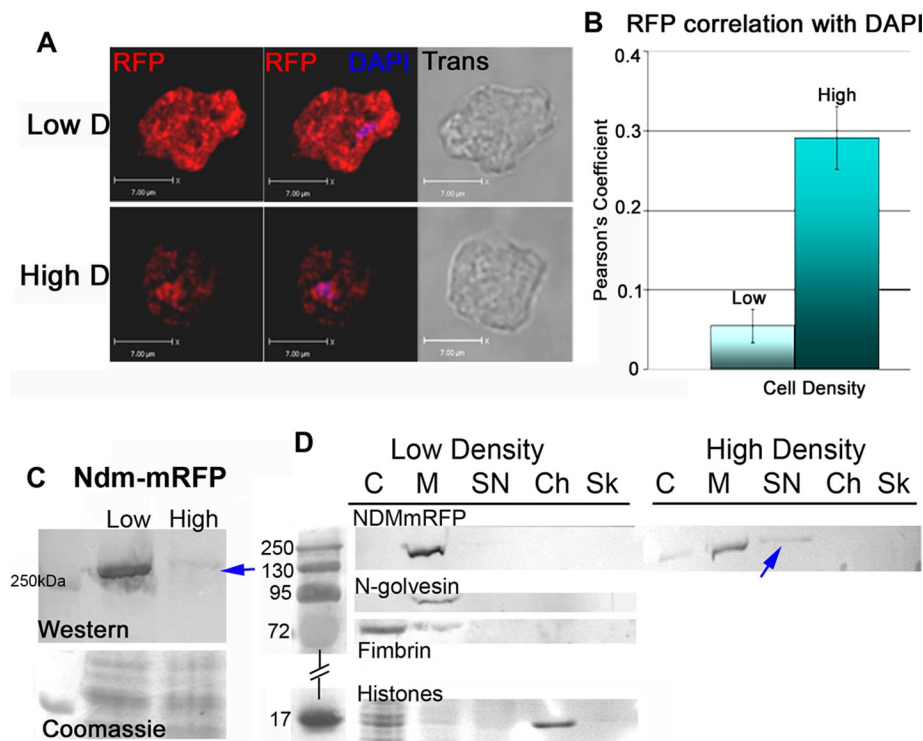
FIGURE 5: Ndm-mRFP expression changes as a function of density and development. (A) Cells growing at low and high densities were placed on coverslips for 15 min, fixed, and stained. Optical sections of cells stained for Ndm-mRFP indirect immunofluorescence (red signal). Overlays with DAPI-stained nuclei (blue) and transmitted images are shown. (B) Pearson coefficient values to determine correlation between Ndm and nuclei colocalization. The entire cell was included in colocalization values. 0, no colocalization; 1, complete colocalization. $n = 30+$ cells at each density from three independent experiments. (C) Western analysis of Ndm-mRFP levels at low and high cell densities (top). The arrow indicates the position of the Ndm-mRFP band. Coomassie staining for protein loading (bottom). (D) Cell fractionation results showing Ndm-mRFP localization in low- and high-density cells. Fractions are as follows: C, cytosol; Ch, chromatin; M, membrane; Sk, cytoskeleton; SN, soluble nuclear. Western blots with anti-RFP antibody (top); controls for protein fractionation (bottom). A blue arrow points out a small but noticeable shift in Ndm-mRFP signal into the soluble nuclear fraction.

products and analyzed by mass spectroscopy. There was significant enrichment of coronin and actin, respectively, in these bands (unpublished data). Mass spectroscopy showed no significant enrichment of coronin or actin with the GBD-formin3 domains or the GST protein alone (unpublished data). This suggests that Ndm can associate with coronin and actin through its CAST domain. Whether this association is direct or indirect is not clear. It could be in a larger complex with other proteins. By contrast to coronin, clathrin, which also shows colocalization with Ndm, was not reproducibly detected in any of the GST pull-down assays.

Ndm had definite effects on macropinocytosis and colocalized with coronin. Coronin is also found in macropinocytosis cups. This raises the question of whether Ndm directly associates with sites of macropinocytosis. To address this, we closely examined F-actin–rich endocytic structures for the presence of Ndm-mRFP (Figure 8B). The F-actin–rich structures on the dorsal surface (opposite the side in contact with the substrate) were mostly devoid of Ndm-mRFP. The absence of Ndm at sites of macropinocytosis suggests an indirect role of Ndm in suppressing endocytosis.

DISCUSSION

Temporal and spatial coordination of protein interactions is vital for actin-driven processes. Many components used in one process can

be reused in another actin-driven process. This likely occurs in the *ndm* signaling pathway, in which Ndm potentially localizes with a general actin-associating protein, coronin, for one process, thereby causing a shift in its function or availability for another process. This shift is important in regulating the actin dynamic processes of cell migration and endocytosis.

Ndm influences migration and endocytosis

Disruption of *ndm* led to a significant increase in the rate of endocytosis and an increase in endocytic cups forming on cells. It is unknown whether the increase is specific to macropinocytosis or whether clathrin-dependent endocytosis may be affected as well. In *ndm*⁻ cells the increase in macropinocytosis was at the expense of rounded lamellipodial protrusions. The *ndm*⁻ cells displayed defects in chemotaxis, extended abnormal pseudopods during migration, and were unable to spread, all lamellipodial-dependent processes.

Evidence of a migration defect was seen during plaque formation, with *ndm*⁻ cells making smaller plaques on bacterial lawns. In addition, the *ndm*⁻ cells formed fewer aggregates during development and smaller fruiting bodies. This suggests difficulties in *ndm*⁻ cells finding their way into aggregation centers. Consistent with these phenotypes, the *ndm*⁻ cells showed a significantly reduced chemotactic index for migration to both folic acid and cAMP. Although it seems likely that increased formation of endocytic cups that break up pseudopodial projections could impair cell movement, the effects on migration rate and directionality were only modestly reduced. The major effect of the *ndm* mutation on cell migration is on the ability to sense the chemoattractant. The increase in endocytosis could increase membrane recycling and interfere with the lifetime of chemoattractant receptors on the cell surface and thus result in the reduction in chemotaxis in the *ndm*⁻ cells.

A lack of cell spreading in *ndm*⁻ cells also suggests a defect in lamellipodial formation (Chamaraux *et al.*, 2005). A decrease in the ability of the cell to organize and extend broad F-actin–rich protrusions was likely responsible for the lack of spreading, especially since there was no difference in cell substrate adhesion. In vertebrate cells a defect in coronin expression inhibited cell spreading (Mishima and Nishida, 1999). The *ndm*⁻ phenotype could mimic the coronin defect in vertebrates because the Ndm/coronin interaction could be essential for localized actin organization and lamellipodia formation necessary for cell spreading.

Ndm and coronin

There was a positive correlation between Ndm localization in the cell and clathrin, coronin, and F-actin localization. Using GST pull downs, we determined Ndm to interact with both coronin and actin. It is possible the interaction with actin was indirect. Because coronin binds actin, it could have been pulled down as a complex. Coronin
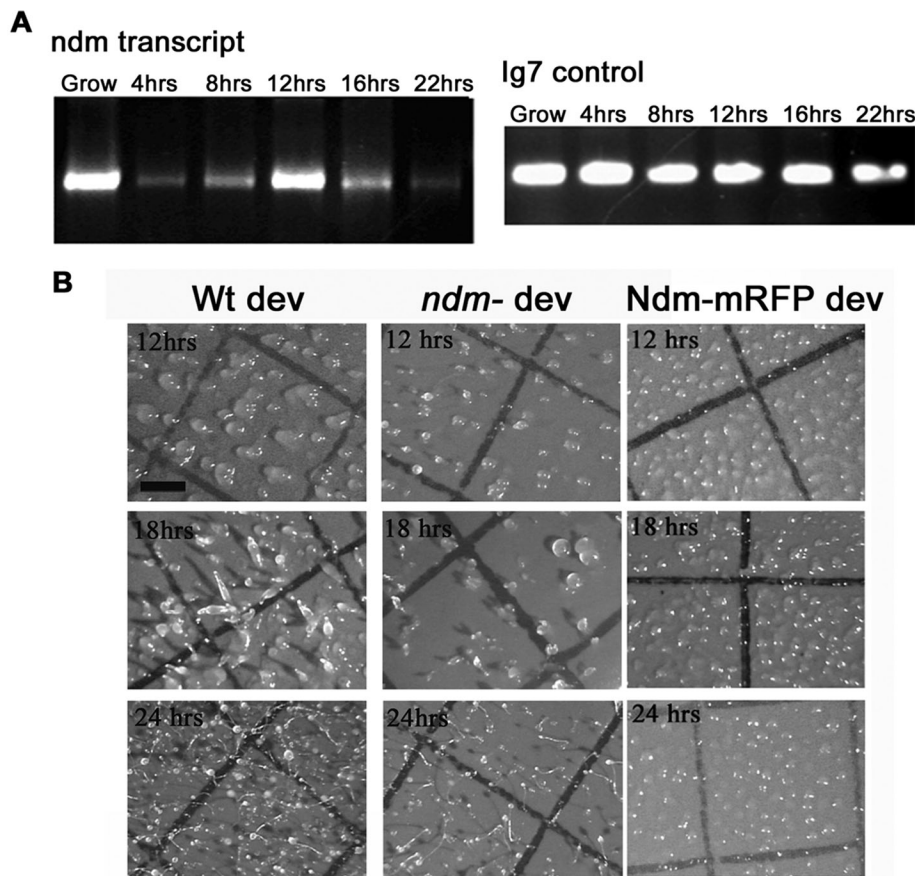
FIGURE 6: Ndm functions in development. (A) RT-PCR showing relative Ndm transcript levels during development. At specific time points RNA was isolated. A cDNA copy of total RNA was used for PCR. *ndm*-specific primers were used to amplify the transcript levels. Ndm transcripts (left) and Ig7 control transcripts (right). (B) Cells were plated for development. Images were taken at the indicated times. WT (left), *ndm*⁻ (center), and Ndm-mRFP (right). Scale bar, 1000 μm.

has been identified in diverse actin dynamic processes in *Dictyostelium*, such as macropinocytosis, phagocytosis, vesicle trafficking, leading-edge formation during migration, and cytokinesis (de Hostos *et al.*, 1991, 1993; Hacker *et al.*, 1997; Rauchenberger *et al.*, 1997). Disruption of coronin results in decreased activity in these actin processes. Coronin has been shown to bind both Arp2/3 and actin. Arp2/3 is an actin nucleator important in creating branched structures. Arp2/3 is controlled by nucleation-promoting factors and is suggested to be regulated by coronin, allowing for appropriate actin cytoskeleton organization (Humphries *et al.*, 2002). Owing to its multiple putative domains, it is possible that Ndm acts as a scaffolding protein interacting with coronin and other proteins.

Dual roles for Ndm?

Ndm localized to membrane fractions, its expression was high at low density, and it was found dispersed throughout the cell and at the cell periphery. At increasing density, protein expression levels decreased and a portion of Ndm localized to the soluble nuclear fraction. Although it involves only a small portion of the Ndm protein, nuclear localization is not unexpected since the Ndm protein contains a nuclear localization signal. The transition of a portion of the Ndm protein from a disperse membrane localization to the nucleus suggests a possibility of dual roles for Ndm—one role directly regulating actin dynamics and another in nuclear functions. It is not uncommon for proteins involved in endocytic pathways to

have dual nuclear functions (Prendergast *et al.*, 2009; Pyrzynska *et al.*, 2009). A small portion of clathrin heavy-chain protein is found in the nucleus. It has been shown to enhance the tumor suppressor protein p53–mediated transcription (Enari *et al.*, 2006). There are also examples of BAR domain–containing proteins with dual actions in endocytosis and nuclear regulations. The BAR domain–containing protein Bin1 was shown to have secondary roles inhibiting transcription of the cMyc oncogene, as well as a role in DNA repair (DuHadaway *et al.*, 2001; Ramalingan *et al.*, 2007). The nucleocytoplasmic protein EhNCABP166 from *Entamoeba histolytica*, like the Ndm protein, contains BAR domains and G-binding, formin 3–homology domains (Campos-Parra *et al.*, 2010). Like Ndm, it also localizes to both the cytoplasm and the nucleus. EhNCABP166 binds F-actin and a number of Rho and Ras GTPases and associates with different phospholipids. It was found to be important for phagocytosis and chemotaxis, although no nuclear roles were established (Campos-Parra *et al.*, 2010).

How does Ndm act?

Ndm was never clearly detected at endocytic cups but is in the poles of moving cells associating with F-actin–rich pseudopodial extensions. The increase in endocytic cups seen in moving cells is at the expense of F-actin–rich, leading-edge lamellipodial extensions. Based on these observations, it seems likely Ndm indirectly inhibits macropinocytosis but has a direct role in proper leading-edge lamellipodial extensions. This role could be similar to the I-BAR–containing protein MIM, which, when disrupted, increases endocytosis and decreases directional migration (Quinones *et al.*, 2010). MIM is suggested to regulate cell movement by inhibiting endocytosis. It does so by binding cortactin, a protein essential for both migration and endocytosis. By binding cortactin, MIM limits the ability of other proendocytic proteins to bind cortactin. Ndm could also be involved in a competition for promigrational or proendocytic proteins. Possibly by associating with coronin, Ndm targets it for lamellipodial formation during migration and restricts its use for endocytosis.

Ndm in vesicle trafficking?

Based on immunofluorescence results, there is some colocalization between Ndm and clathrin. Another result suggesting Ndm interaction during early endocytic events is its association with phosphatidylinositol-3-phosphates (PI3Ps; Supplemental Figure S4). These lipids are enriched in early endosomes and are important for endosome internalization (Petiot *et al.*, 2003). Recently a BAR domain–containing protein in *Dictyostelium*, IBARa, was found to colocalize to regions of clathrin puncta and was suggested to be involved in clathrin-mediated endocytosis and vesicle trafficking (Veltman *et al.*, 2011). PI3Ps are key in determining the flow of endosomal transport, from early endosomes to later stages of degradation or recycling (Fili *et al.*, 2006). The clathrin colocalization and PI3P association of
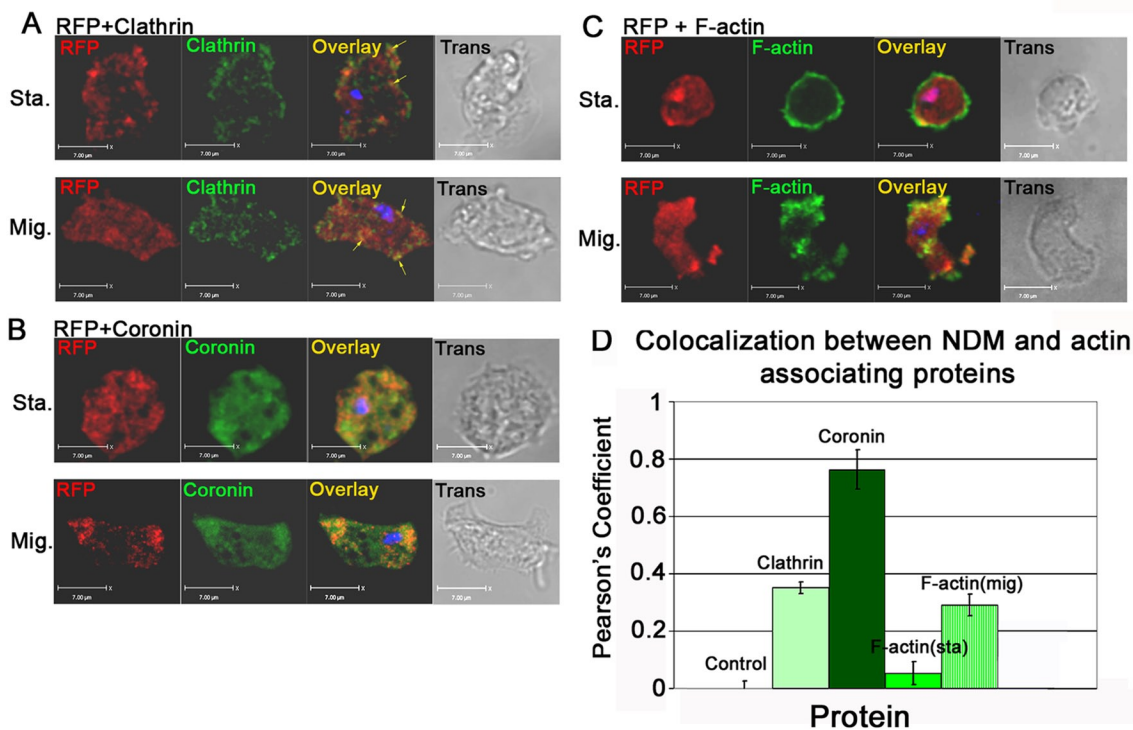
FIGURE 7: Ndm colocalizes with specific actin-associating proteins. Low-density growing cells were placed on a coverslip, fixed, and stained. Fixation was either immediately after placing the growing cells on the coverslip (stationary [Sta.]) or after cells were induced to migrate to folic acid (Mig.). Left, Ndm-mRFP indirect immunofluorescence (red); middle, other protein antibodies (green); right, transmitted light images. (A) Clathrin, (B) coronin, and (C) phalloidin staining F-actin. Yellow arrows in A indicate points of clathrin and Ndm colocalization. Images are optical sections. Nuclei were stained with DAPI (blue). Yellow/orange signal indicates colocalization in the overlays. (E) Colocalization is indicated by a positive Pearson's coefficient. The entire cell was included in colocalization values. Colocalization of F-actin with DAPI was used as a negative control to represent 0 correlation. Complete colocalization gives a coefficient of 1. F-Actin colocalization was measured with Ndm-mRFP in both stationary (Sta.) and migrating (Mig.) cells. $n = 30+$ cells from at least two independent experiments.

Ndm raises the possibility of a role in vesicle trafficking. Could clathrin assist Ndm in the vesicle trafficking of coronin to specific sites of front-end, actin-rich lamellipodial formations (Lau and Chou, 2008)?

MATERIALS AND METHODS
Dictyostelium growth and development
Wild-type (AX3), *ampAOE* (G418 resistant), or *ampA*⁻ (originally blasticidin resistant, but the blasticidin resistance cassette was removed via cre-loxP recombination; Kimmel and Faix, 2006) cells were grown as previously described (Sussman, 1987). Transformed cell lines were grown in 9.6 μg/ml G418 or 10μg/ml blasticidin S for selection. For growth over bacteria, cells were plated with *E. coli* B/r on LP agar plates (Oyama and Blumberg, 1986). For cell growth, low density was ~1 × 10⁶ cells/ml and high density was (exponential log growth) 2 × 10⁶ to 5 × 10⁶ cells/ml. Cells were starved on filters to induce development (Eichinger and Rivero, 2010).

DNA preparation
DNA preparation was performed as described (Nellen *et al.*, 1987)

Cell fractionation
Fractionation used the Thermo Scientific (Waltham, MA) subcellular protein fractionation kit according to the manufacturer's instructions and as described in Kelsey *et al.* (2012). Controls used were a strain containing the membrane-localizing N-golvesin GFP, the fimbrin

antibody to detect soluble fimbrin localization, and the histone location as detected by Coomassie staining (Kelsey *et al.*, 2012).

REMI mutagenesis and gene identification
REMI mutagenesis was adapted from Shaulsky *et al.* (1996) and Kuspa (2006) as described in Kelsey *et al.* (2012).

ndm⁻ cell strains
The original REMI plasmid with flanking *ndm* genomic DNA linearized with *Cla*I was used to create knockout strains in wild-type, *ampAOE*, and *ampA*⁻ backgrounds. To verify insertion of the REMI plasmid into the DDB_G0272368/*ndm* gene, we used the following primers in PCRs with genomic DNA: forward, 5'-ATGAATAAAGACCAACATGAAA-3'; and reverse, 5'-GTTCTT-GTAATTGTTGGATTTCAATC-3'. These primers flank the expected site of insertion in the gene, and they produced a 638–base pair fragment in WT cells and a 5000–base pair fragment when the pGEM3-bsr REMI plasmid insert is present (Figure 1H).

Ndm-mRFP construction
The Ndm-mRFP plasmid (Supplemental Figure S2) contains 1260 base pairs of the 3' end of the *ndm* coding region and 1252 base pairs of 3' *ndm* noncoding region sequence immediately downstream of the *ndm* termination site. The plasmid was designed to incorporate a proline–alanine linker (32 base pairs). The linker is
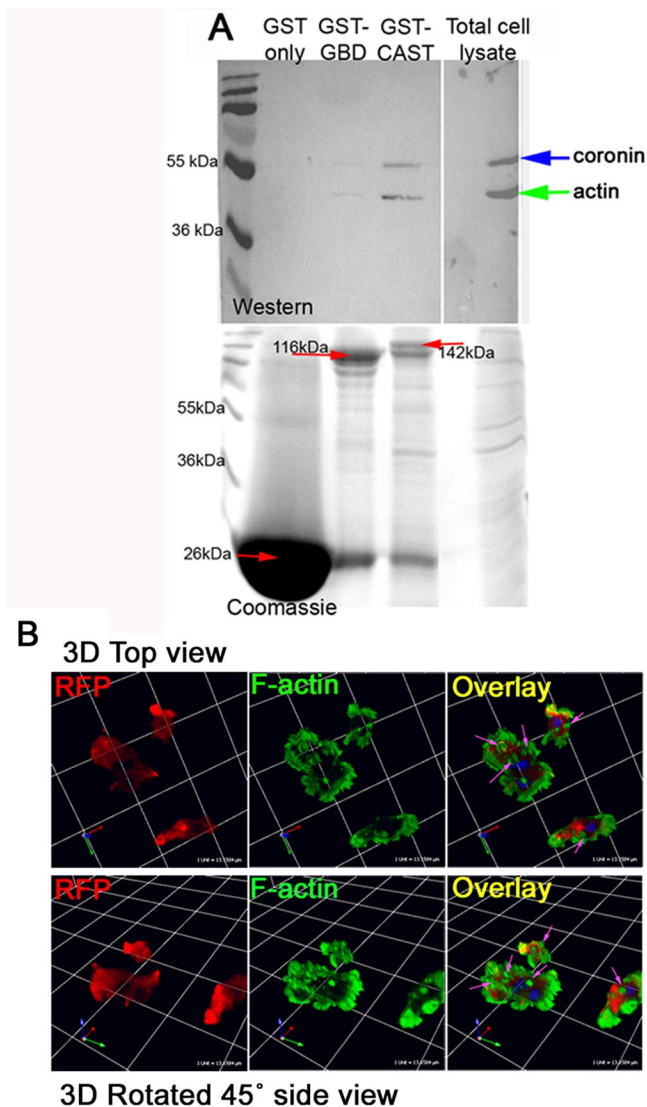
FIGURE 8: Interaction of Ndm with coronin and actin. Ndm is not found at sites of macropinocytosis. (A) Western blot incubated with both anti-coronin and anti-actin antibodies (top); Coomassie staining (bottom). Lanes contain (from left) a molecular weight ladder, GST-only incubation with cell lysate, GST-GBD incubation with cell lysate, GST-CAST incubation with cell lysate, and a sample of total cell lysate shown as a reference. The blue arrow marks coronin at 55 kDa; the green arrow marks actin at 45 kDa. In the Coomassie-stained gel, GST fusion proteins are visible, GST (26 kDa), GST-GBD (116 kDa), and GST-CAST (142 kDa). (B) Growing cells expressing Ndm-mRFP were fixed and stained for RFP and F-actin localization. Three-dimensional reconstructed images of cells are shown for a better view of dorsal endocytic cup formations. Top, a top view looking down at the cells. Bottom, a side view rotated slightly. Ndm-mRFP localization (left), F-actin staining (center), and overlays (right). Endocytic cup structures are indicated by pink arrows in the overlay images.

followed in-frame by the mRFPmars coding sequence at the carboxy terminus of the protein (Müller-Taubenberger et al., 2006). Following the mRFPmars coding region is a 270–base pair terminator sequence from the 3′ noncoding region of the ampA gene. The plasmid also contains the floxed bsr cassette for selection (Kimmel and Faix, 2006). For 3′ coding region amplification and linker addition the PCR primers used were as follows: forward, 5′-CAGGGGGC-

CCTCGAAACTCGATGAAATGATTCAAG-3′; and reverse, 5′-CAG-GTCGACCCTGCACCTGCACCTGCACCTGCACCTGTT-GTTGTAGTTGTTGTAGTTGT-3′. The primers produce a 1260–base pair product containing the 3′ coding region plus the linker.

For the 3′ noncoding region the primers used were as follows: forward, 5′-CAGGCGGCCGCGAGGTACTGGTTGTTGGTAAGT-GTTG-3′; and reverse, 5′-CAGCCGCGGGCAGCAGAAGCATTTAA-AGAAATAGC-3z. The primers produce a 1252–base pair fragment. The plasmid was linearized with ApaI and SacII before electroporation. Electroporation is described in Kelsey et al. (2012).

The primers used to verify insertion into the ndm gene were as follows: forward, 5′- CCATTTCAATCAACTACAACTAC-3′; and reverse, 5′-TAACAGTAGAATGTTAAGACCAC-3′. The primers produce a 300–base pair product in wild-type DNA and a 2600–base pair product with the ndmRFP construct insertion.

Immunodetection

For Western analysis, protein from 1×10^6 cells was run on 6 or 12% SDS–PAGE gels and transferred to nitrocellulose. A 1:500 dilution of anti-RFP or anti-GFP antibody (5F8 and 3H9, rat; ChromoTek, Martinsried, Germany) and a 1:3000 dilution of anti-rat alkaline phosphatase–conjugated antibody (S383A; Promega, Madison, WI) were used for primary and secondary antibodies, respectively. For GST pull-down identifications, a 1:1000 dilution of anti-actin antibody (mouse, 224-236-1; Developmental Studies Hybridoma Bank, University of Iowa, Iowa City, IA; Westphal et al., 1997) or a 1:750 dilution of anti-coronin antibody (mouse, 176-3-6; Developmental Studies Hybridoma Bank; de Hostos et al., 1991) was used as a primary antibody. An alkaline phosphatase–conjugated goat anti–mouse immunoglobulin G (IgG; Jackson ImmunoResearch Laboratories, West Grove, PA) was used as a secondary.

For indirect immunofluorescence, cells were fixed in 4% formaldehyde in 20 mM NaPO$_4$ and permeabilized in methanol with 1% formaldehyde. Primary antibodies were diluted in 1% bovine serum albumin at 1:300 for anti-RFP or anti-GFP (same as Western), 1:300 anti-clathrin heavy chain (rabbit antibody P1663; Cell Signaling Technology, Beverly, MA), 1:50 anti-coronin (mouse antibody 176-2-5; Developmental Studies Hybridoma Bank; de Hostos et al., 1991), 1: 50 anti-fimbrin (antibody 210-183-1; Developmental Studies Hybridoma Bank; Prassler et al., 1998), and 1:50 anti-p80 (H161; Developmental Studies Hybridoma Bank; Ravanel et al., 2001). For DAPI staining, cells were incubated for 10 min in a 25 ng/ml DAPI solution (AnaSpec, Fremont, CA). In the case of dextran endocytosis, cells were incubated in HL5 plus fluorescein isothiocyanate–dextran (molecular weight, 20,000; Sigma-Aldrich, St. Louis, MO) at 2 mg/ml for 1 h before fixation. Secondary antibodies used were 1:200 dilutions of goat anti–rat, donkey anti–rabbit, or goat anti–mouse 488 or 594 Alexa Fluor conjugated (Molecular Probes, Eugene, OR).

For actin staining, cells were fixed in 0.3% glutaraldehyde and permeabilized with 0.1% Triton X-100 in phosphate-buffered saline buffer, pH 7.4. Where used, primary antibodies were applied, followed by incubation with secondary antibodies. Alexa Fluor 488–phalloidin (Molecular Probes) at a 1:500 dilution was included in the secondary incubation to label F-actin. Alexa Fluor 594–conjugated deoxyribonuclease I (Molecular Probes) was added along with the phalloidin to label unpolymerized G-actin.

Microscopy

A Leica (Wetzlar, Germany) SP5 scanning confocal light microscope was used for imaging. Conditions are described in Kelsey et al. (2012). Volocity software 5.5 (PerkinElmer, Waltham, MA) was used

to assemble images and calculate Pearson's coefficient of correlation (Barlow *et al.*, 2010). Agar plates were viewed under an Olympus (Tokyo, Japan) dissecting scope. Images were obtained using a DC330 video camera (DAGE-MTI, Michigan City, IN). Images used for calculating plaque sizes were processed and analyzed using MetaMorph, version 7.0r1 (Molecular Devices, Sunnyvale, CA).

Chemotaxis

The procedure for folic acid chemotaxis was adapted from Hadwiger and Srinivasan (1999), except that cells were deposited on very thin layers of agar on chambered coverslips. For cAMP chemotaxis cells were starved for 6 h at 22°C on filters. Details are described in Kelsey *et al.* (2012). Velocity and directionality values were obtained using the manual tracking (http://rsb.info.nih.gov/ij/plugins/track) and chemotaxis tools (www.ibidi.de/applications/ap_chemo.html) on ImageJ (National Institutes of Health, Bethesda, MD). Directionality is defined as the Euclidean distance traveled between the start point and the end point divided by the total distance traveled. The chemotactic index (CI) is equal to the cosine of the angle formed between the line of movement of the cell and the line representing direct movement to the chemoattractant. The slope of individual cell movements (from ImageJ) was used to determine the angle and CI value. Using the slope, we calculated the angle from the origin by taking the antitangent. By subtracting that angle from the angle of placement of the chemoattractant, the angle difference between the two paths is established. Taking the cosine of the angle of difference gives the chemotactic index.

Dextran endocytosis

For imaging live dextran endocytosis, cells were incubated in HL5 plus fluorescein isothiocyanate–dextran (molecular weight, 20,000; 2 mg/ml; Sigma-Aldrich,) for 1 h before visualization on a Leica SP5 confocal microscope. The procedure for measuring rates of endocytosis and exocytosis was from Brazill *et al.* (2001). A VersaFluor fluorometer (Bio-Rad, Hercules, CA) with 488-nm excitation and 520-nm emission filters was calibrated with a set of controls and used to measure FITC fluorescence.

RT-PCR

RNA from 1×10^7 cells was isolated according to TRIzol reagent protocol (15596-018; Invitrogen, Carlsbad, CA). First-strand cDNA synthesis kit (Fermentas, Glen Burnie, MD) was used to create cDNA from the RNA. PCR amplification of the first-strand cDNA used a standard Taq (Fermentas) procedure and primers designed for the specific amplification. *ndm* primers used in RT-PCR were the 3′ coding primers used in mRFP plasmid construction—5′- TCGAAACTC-GATGAAATGATTCAAG-3′and5′-GTTGTTGTAGTTGTTGTAGTTGT-3′—which yielded a 1206–base pair fragment. As a control, Ig7 primers were used—5′- TTACATTTATTAGACCCGAAACCAAGCG-3′ and 5′-TTCCCTTTAGACCTATGGACCTTAGCG-3′—which yielded a 370–base pair fragment (Hopper *et al.*, 1993). A gel doc digital imaging system (IS-100; Alpha Innotech, San Leandro, CA) was used to quantify band intensity under conditions in which the signal was linearly dependent on the amount of material loaded. Unequal protein loading or unequal RNA levels were taken into account with the Coomassie and Ig7 controls. The relative intensity of the bands was calculated, with the most intense band set equal to 100%.

GST fusion protein construction and analysis

GST fusions were constructed by amplifying regions of the *ndm* gene using the following primer sets: GST-GBD, forward, 5′-GCGCGGATC-CTATTTATTGCAATCTAATAAGG-3′, and reverse, 5′-CGCGCTC-GAGTTATTGATATTGTTGTTTTTC-3′; GST-CAST, forward 5′- GCGG-GATCCACAATTCAAGAATTTCAAG-3′, and reverse, 5′-CGCGCTC-GAGTTACAATTGAATAGTTGAG-3′. Each forward primer contains a *Bam*HI restriction enzyme cut site, and each reverse primer contains an *Xho*I restriction enzyme cut site.

Gene segments were cloned into a pGEX-6P-1 vector (GE Healthcare, Piscataway, NJ) and transformed into BL21 (DE3) *E. coli* cells. The pGEX-6P-1 contains a tac promoter and lacl[q] gene for inducible expression by isopropyl β-D-1-thiogalactopyranoside and also a GST fusion protein tag for placement on the N-terminus of each protein segment. The procedure for expression and isolation of fusion proteins and the pull-down assay was from Kae *et al.* (2004) with the French press step omitted. The GST-GBD fusion protein was 116 kDa, and the GST-CAST fusion produced a protein product of 142 kDa.

The standard PIP strips (P-6001; Echelon Bioscience, Salt Lake City, UT) procedure was followed (Dowler *et al.*, 2002). An amount of 1.5 µg/ml protein was used for all GST fusion protein incubations. The anti-GST antibody was a rabbit polyclonal anti-GST (ab9085; Abcam, Cambridge, MA) used at a concentration of 1:2000. The secondary antibody was an alkaline phosphatase–conjugated, goat anti–rabbit IgG (Jackson ImmunoResearch Laboratories). PI(4,5)P2 Grip (G-4501; Echelon), which recognizes phosphatidylinositol 4,5-bisphosphate, was used as a positive control at a concentration of 0.5 µg/ml (Kavran *et al.*, 1998).

Statistical analysis

p values were calculated using the paired two-sample test on Excel (Microsoft, Redmond, WA). $p \leq 0.05$ was deemed significant.

REFERENCES

Affolter M, Weijer CJ (2005). Signaling to cytoskeletal dynamics during chemotaxis. Dev Cell 9, 19–34.

Barlow AL, Macleod A, Noppen S, Sanderson J, Guérin CJ (2010). Colocalization analysis in fluorescence micrographs: verification of a more accurate calculation of Pearson's correlation coefficient. Microsc Microanal 16, 710–724.

Blumberg DD, Ho HN, Petty CL, Varney TR, Gandham S (2002). AmpA, a modular protein containing disintegrin and ornatin domains, has multiple effects on cell adhesion and cell fate specification. J Muscle Res Cell Motil 23, 817–828.

Brazill DT, Meyer LR, Hatton RD, Brock DA, Gomer RH (2001). ABC transporters required for endocytosis and endosomal pH regulation in *Dictyostelium*. J Cell Sci 114, 3923–3932.

Campos-Parra AD, Hernández-Cuevas NA, Hernandez-Rivas R, Vargas M (2010). EhNCABP166: a nucleocytoplasmic actin-binding protein from *Entamoeba histolytica*. Mol Biochem Parasitol 172, 19–30.

Casademunt E, Varney T, Dolman J, Petty C, Blumberg D (2002). A gene encoding a novel anti-adhesive protein is expressed in growing cells

and restricted to anterior-like cells during development of *Dictyostelium*. Differentiation 70, 23–35.

Chamaraux F, Fache S, Bruckert F, Fourcade B (2005). Kinetics of cell spreading. Phys Rev Lett 94, 158102.

Collins A, Warrington A, Taylor KA, Svitkina T (2011). Structural organization of the actin cytoskeleton at sites of clathrin-mediated endocytosis. Curr Biol 21, 1167–1175.

de Hostos EL (1999). The coronin family of actin-associated proteins. Trends Cell Biol 9, 345–350.

de Hostos EL, Bradtke B, Lottspeich F, Guggenheim R, Gerisch G (1991). Coronin, an actin binding protein of *Dictyostelium discoideum* localized to cell surface projections, has sequence similarities to G protein beta subunits. EMBO J 10, 4097–4104.

de Hostos EL, Rehfuess C, Bradtke B, Waddell DR, Albrecht R, Murphy J, Gerisch G (1993). *Dictyostelium* mutants lacking the cytoskeletal protein coronin are defective in cytokinesis and cell motility. J Cell Biol 120, 163–173.

Deken SL, Vincent R, Hadwiger G, Liu Q, Wang ZW, Nonet ML (2005). Redundant localization mechanisms of RIM and ELKS in *Caenorhabditis elegans*. J Neurosci 25, 5975–5983.

Dowler S, Kular G, Alessi DR (2002). Protein lipid overlay assay. Sci STKE 2002, pl6.

DuHadaway JB, Sakamuro D, Ewert DL, Prendergast GC (2001). Bin1 mediates apoptosis by c-Myc in transformed primary cells. Cancer Res 61, 3151–3156.

Eichinger L, Rivero F (2010). *Dictyostelium discoideum* Protocols, Totowa, NJ: Humana Press.

Enari M, Ohmori K, Kitabayashi I, Taya Y (2006). Requirement of clathrin heavy chain for p53-mediated transcription. Genes Dev 20, 1087–1099.

Fili N, Calleja V, Woscholski R, Parker PJ, Larijani B (2006). Compartmental signal modulation: endosomal phosphatidylinositol 3-phosphate controls endosome morphology and selective cargo sorting. Proc Natl Acad Sci USA 103, 15473–15478.

Frost A, Unger VM, De Camilli P (2009). The BAR domain superfamily: membrane-molding macromolecules. Cell 137, 191–196.

Gandhi M, Achard V, Blanchoin L, Goode BL (2009). Coronin switches roles in actin disassembly depending on the nucleotide state of actin. Mol Cell 34, 364–374.

Gerisch G, Albrecht R, Heizer C, Hodgkinson S, Maniak M (1995). Chemoattractant-controlled accumulation of coronin at the leading edge of *Dictyostelium* cells monitored using a green fluorescent protein-coronin fusion protein. Curr Biol 5, 1280–1285.

Girao H, Geli MI, Idrissi FZ (2008). Actin in the endocytic pathway: from yeast to mammals. FEBS Lett 582, 2112–2119.

Graham TR, Kozlov MM (2010). Interplay of proteins and lipids in generating membrane curvature. Curr Opin Cell Biol 22, 430–436.

Hacker U, Albrecht R, Maniak M (1997). Fluid-phase uptake by macropinocytosis in *Dictyostelium*. J Cell Sci 110, 105–112.

Hadwiger JA, Srinivasan J (1999). Folic acid stimulation of the Galpha4 G protein-mediated signal transduction pathway inhibits anterior prestalk cell development in *Dictyostelium*. Differentiation 64, 195–204.

Hopper NA, Harwood AJ, Bouzid S, Véron M, Williams JG (1993). Activation of the prespore and spore cell pathway of *Dictyostelium* differentiation by cAMP-dependent protein kinase and evidence for its upstream regulation by ammonia. EMBO J 12, 2459–2466.

Humphries CL, Balcer HI, D'Agostino JL, Winsor B, Drubin DG, Barnes G, Andrews BJ, Goode BL (2002). Direct regulation of Arp2/3 complex activity and function by the actin binding protein coronin. J Cell Biol 159, 993–1004.

Insall RH, Machesky LM (2009). Actin dynamics at the leading edge: from simple machinery to complex networks. Dev Cell 17, 310–322.

Insall R, Müller-Taubenberger A, Machesky L, Köhler J, Simmeth E, Atkinson SJ, Weber I, Gerisch G (2001). Dynamics of the *Dictyostelium* Arp2/3 complex in endocytosis, cytokinesis, and chemotaxis. Cell Motil Cytoskeleton 50, 115–128.

Janetopoulos C, Firtel RA (2008). Directional sensing during chemotaxis. FEBS Lett 582, 2075–2085.

Kae H, Lim CJ, Spiegelman GB, Weeks G (2004). Chemoattractant-induced Ras activation during *Dictyostelium* aggregation. EMBO Rep 5, 602–606.

Kaeser PS, Deng L, Chávez AE, Liu X, Castillo PE, Südhof TC (2009). ELKS2alpha/CAST deletion selectively increases neurotransmitter release at inhibitory synapses. Neuron 64, 227–239.

Kavran JM, Klein DE, Lee A, Falasca M, Isakoff SJ, Skolnik EY, Lemmon MA (1998). Specificity and promiscuity in phosphoinositide binding by pleckstrin homology domains. J Biol Chem 273, 30497–30508.

Kelsey JS, Fasman NM, Blumberg DD (2012). Evidence of an evolutionarily conserved LMBR1 domain-containing protein that associates with endocytic cups and plays a role in cell migration in *Dictyostelium discoideum*. Eukaryotic Cell 11, 401–416.

Kimmel AR, Faix J (2006). Generation of multiple knockout mutants using the Cre-loxP system. Methods Mol Biol 346, 187–199.

Kuspa A (2006). Restriction enzyme-mediated integration (REMI) mutagenesis. Methods Mol Biol 346, 201–209.

Lau AW, Chou MM (2008). The adaptor complex AP-2 regulates post-endocytic trafficking through the non-clathrin Arf6-dependent endocytic pathway. J Cell Sci 121, 4008–4017.

Machesky LM, Insall RH (1998). Scar1 and the related Wiskott-Aldrich syndrome protein, WASP, regulate the actin cytoskeleton through the Arp2/3 complex. Curr Biol 8, 1347–1356.

Machesky LM, Reeves E, Wientjes F, Mattheyse FJ, Grogan A, Totty NF, Burlingame AL, Hsuan JJ, Segal AW (1997). Mammalian actin-related protein 2/3 complex localizes to regions of lamellipodial protrusion and is composed of evolutionarily conserved proteins. Biochem J 328, 105–112.

May RC, Machesky LM (2001). Phagocytosis and the actin cytoskeleton. J Cell Sci 114, 1061–1077.

Mishima M, Nishida E (1999). Coronin localizes to leading edges and is involved in cell spreading and lamellipodium extension in vertebrate cells. J Cell Sci 112, 2833–2842.

Müller-Taubenberger A, Vos MJ, Böttger A, Lasi M, Lai FP, Fischer M, Rottner K (2006). Monomeric red fluorescent protein variants used for imaging studies in different species. Eur J Cell Biol 85, 1119–1129.

Nellen W, Datta S, Reymond C, Sivertsen A, Mann S, Crowley T, Firtel R (1987). Molecular biology in *Dictyostelium*: tools and applications. Methods Cell Biol 28, 67–100.

Nikolaev Y, Pervushin K (2009). Rethinking leucine zipper—a ubiquitous signal transduction motif. Nature Proceedings Available at: http://hdl.handle.net/10101/npre.2009.3271.1 (accessed 2009).

Noegel AA, Schleicher M (2000). The actin cytoskeleton of *Dictyostelium*: a story told by mutants. J Cell Sci 113, 759–766.

O'Halloran TJ, Anderson RG (1992). Clathrin heavy chain is required for pinocytosis, the presence of large vacuoles, and development in *Dictyostelium*. J Cell Biol 118, 1371–1377.

Oyama M, Blumberg D (1986). Changes during differentiation in requirements of cAMP for expression of cell-type-specific mRNAs in the cellular slime mold, *Dictyostelium discoideum*. Dev Biol 117, 550–556.

Pagni M, Ioannidis V, Cerutti L, Zahn-Zabal M, Jongeneel CV, Hau J, Martin O, Kuznetsov D, Falquet L (2007). MyHits: improvements to an interactive resource for analyzing protein sequences. Nucleic Acids Res 35, W433–W437.

Petersen J, Nielsen O, Egel R, Hagan IM (1998). FH3, a domain found in formins, targets the fission yeast formin Fus1 to the projection tip during conjugation. J Cell Biol 141, 1217–1228.

Petiot A, Faure J, Stenmark H, Gruenberg J (2003). PI3P signaling regulates receptor sorting but not transport in the endosomal pathway. J Cell Biol 162, 971–979.

Prassler J, Murr A, Stocker S, Faix J, Murphy J, Marriott G (1998). DdLIM is a cytoskeleton-associated protein involved in the protrusion of lamellipodia in *Dictyostelium*. Mol Biol Cell 9, 545–559.

Prendergast GC, Muller AJ, Ramalingam A, Chang MY (2009). BAR the door: cancer suppression by amphiphysin-like genes. Biochim Biophys Acta 1795, 25–36.

Pyrzynska B, Pilecka I, Miaczynska M (2009). Endocytic proteins in the regulation of nuclear signaling, transcription and tumorigenesis. Mol Oncol 3, 321–338.

Quinones GA, Jin J, Oro AE (2010). I-BAR protein antagonism of endocytosis mediates directional sensing during guided cell migration. J Cell Biol 1 89, 353–367.

Ramalingam A, Farmer GE, Stamato TD, Prendergast GC (2007). Bin1 interacts with and restrains the DNA end-binding protein complex Ku. Cell Cycle 6, 1914–1918.

Rauchenberger R, Hacker U, Murphy J, Niewöhner J, Maniak M (1997). Coronin and vacuolin identify consecutive stages of a late, actin-coated endocytic compartment in *Dictyostelium*. Curr Biol 7, 215–218.

Ravanel K, de Chassey B, Cornillon S, Benghezal M, Zulianello L, Gebbie L, Letourneur F, Cosson P (2001). Membrane sorting in the endocytic and phagocytic pathway of *Dictyostelium discoideum*. Eur J Cell Biol 80, 754–764.

Rivero F, Somesh BP (2002). Signal transduction pathways regulated by Rho GTPases in *Dictyostelium*. J Muscle Res Cell Motil 23, 737–749.

Rivero F, Muramoto T, Meyer AK, Urushihara H, Uyeda TQ, Kitayama C (2005). A comparative sequence analysis reveals a common GBD/FH3-FH1-FH2-DAD architecture in formins from *Dictyostelium*, fungi and metazoa. BMC Genomics 6, 28.

Roy A, Kucukural A, Zhang Y (2010). I-TASSER: a unified platform for automated protein structure and function prediction. Nat Protoc 5, 725–738.

Salazar MA, Kwiatkowski AV, Pellegrini L, Cestra G, Butler MH, Rossman KL, Serna DM, Sondek J, Gertler FB, De Camilli P (2003). Tuba, a novel protein containing bin/amphiphysin/Rvs and Dbl homology domains, links dynamin to regulation of the actin cytoskeleton. J Biol Chem 278, 49031–49043.

Shaulsky G, Escalante R, Loomis WF (1996). Developmental signal transduction pathways uncovered by genetic suppressors. Proc Natl Acad Sci USA 93, 15260–15265.

Soll D (2003). *Dictyostelium* may model diseases involving defects in cellular chemotaxis. ASM News 69, 246.

Suetsugu S (2010). The proposed functions of membrane curvatures mediated by the BAR domain superfamily proteins. J Biochem 148, 1–12.

Sussman M (1987). Cultivation and synchronous morphogenesis of *Dictyostelium* under controlled experimental conditions. Methods Cell Biol 28, 9–29.

Uetrecht AC, Bear JE (2006). Coronins: the return of the crown. Trends Cell Biol 16, 421–426.

Varney T, Casademunt E, Ho H, Petty C, Dolman J, Blumberg D (2002a). A novel *Dictyostelium* gene encoding multiple repeats of adhesion inhibitor-like domains has effects on cell-cell and cell-substrate adhesion. Dev Biol 243, 226–248.

Varney T, Ho H, Petty C, Blumberg D (2002b). A novel disintegrin domain protein affects early cell type specification and pattern formation in *Dictyostelium*. Development 129, 2381–2389.

Veltman DM, Auciello G, Spence HJ, Machesky LM, Rappoport JZ, Insall RH (2011). Functional analysis of *Dictyostelium* IBARa reveals a conserved role of the I-BAR domain in endocytosis. Biochem J 436, 45–52.

Wang Q, Navarro MV, Peng G, Molinelli E, Goh SL, Judson BL, Rajashankar KR, Sondermann H (2009). Molecular mechanism of membrane constriction and tubulation mediated by the F-BAR protein pacsin/syndapin. Proc Natl Acad Sci USA 106, 12700–12705.

Washington RW, Knecht DA (2008). Actin binding domains direct actin-binding proteins to different cytoskeletal locations. BMC Cell Biol 9, 10.

Westphal M, Jungbluth A, Heidecker M, Mühlbauer B, Heizer C, Schwartz JM, Marriott G, Gerisch G (1997). Microfilament dynamics during cell movement and chemotaxis monitored using a GFP-actin fusion protein. Curr Biol 7, 176–183.